Earth System
Dynamics
Discussions

A Dynamical Systems Characterisation of Atmospheric Jet Regimes

Gabriele Messori[1,2,*], Nili Harnik[3,*], Erica Madonna[4,5], Orli Lachmy[6], and Davide Faranda[7,8,9]

[1]Department of Earth Sciences, Uppsala University, Uppsala, Sweden.
[2]Department of Meteorology and Bolin Centre for Climate Research, Stockholm University, Stockholm, Sweden
[3]Department of Geosciences, Tel Aviv University, Tel Aviv, Israel.
[4]Geophysical Institute, University of Bergen, Bergen, Norway
[5]Bjerknes Centre for Climate Research, Bergen, Norway
[6]Department of Natural Sciences, Open University of Israel, Ra'anana, Israel
[7]Laboratoire des Sciences du Climat et de l'Environnement, LSCE/IPSL, CEA-CNRS-UVSQ, Université Paris-Saclay, Gif-sur-Yvette, France.
[8]London Mathematical Laboratory, London, U. K.
[9]LMD/IPSL, Ecole Normale Superieure, PSL research University, Paris, France
[*]The authors have contributed equally to the manuscript

Correspondence: Gabriele Messori (gabriele.messori@geo.uu.se)

Abstract. Atmospheric jet streams are typically separated into primarily "eddy-driven", or "polar-front" jets and primarily "thermally-driven", or "subtropical" jets. Some regions also display "merged" jets, resulting from the (quasi) co-location of the regions of eddy generation with the subtropical jet. The different locations and driving mechanisms of these jets issue from very different underlying mechanisms, and result in very different jet characteristics. Here, we link our understanding of the dynamical jet maintenance mechanisms, mostly issuing from conceptual or idealised models, to the phenomena observed in reanalysis data. We specifically focus on developing a unitary analysis framework, grounded in dynamical systems theory, which may be applied to both idealised model and reanalysis data, and allow for direct intercomparison. Our results provide a proof-of-concept for using dynamical systems indicators to diagnose jet regimes in a versatile, conceptually intuitive and computationally efficient fashion.

1 Introduction

To zeroth-order, the global atmospheric circulation may be construed as arising from the three-way interaction between the mean meridional circulation, mid-latitude zonal jet streams and baroclinically unstable eddies. Advection of planetary angular momentum by the mean meridional circulation, and specifically by the thermally direct Hadley cell, supports the so-called "thermally-driven" jets (Held and Hou, 1980). Convergence of eddy momentum flux by baroclinc eddies supports the so-called "eddy-driven" jets (Held, 1975; Rhines, 1975). Purely thermally-driven or eddy-driven jets are largely theoretical constructs: the former would require an eddy-less, axisymmetric atmosphere (Held and Hou, 1980), while the latter can only exist in the

absence of advection of planetary momentum (e.g., Panetta, 1993). However, there are atmospheric flows that approximate to a good degree these two limiting cases. These are often termed "subtropical" and "polar-front" jets, in reference to their

20   geographical locations.

The subtropical jet is an upper tropospheric jet with a strong vertical shear, located at the poleward edge of the Hadley Cell. While the observed tropical circulation is distinctly zonally asymmetric (e.g., Heaviside and Czaja, 2013), the underlying physical drivers of this flow may be related to the idealised axisymmetric scenario of Held and Hou (1980). To the north of the Hadley Cell, the Ferrel Cell corresponds to a region of strong baroclinic activity. Here, an equivalent barotropic polar-front jet

25   exists (e.g., Hoskins et al., 1983). While the advection of planetary momentum in the region is clearly non-zero, we can again relate this jet to one of the idealised limiting cases described above. Specifically, two-layer quasi-geostrophic models show that in this region, when a geophysical background flow is perturbed, the growing baroclinc waves that result from the perturbations can spontaneously generate a jet by converging westerly momentum flux (e.g., Panetta, 1993; Lee, 1997).

The distinction between the subtropical and polar-front jets is not always evident, and the jets display different character-

30   istics depending on geographical location and season. In the Northern Hemisphere, the two flows are mostly separate during wintertime over the North Atlantic basin, while over parts of Asia and the Pacific the default atmospheric configuration is of a single, or "merged" jet. This terminology is supported by evidence that the single jet results from the (quasi) co-location of the regions of eddy generation with the subtropical jet, such that the driving mechanisms are both thermal and eddy-related (Eichelberger and Hartmann, 2007; Li and Wettstein, 2012; O'Rourke and Vallis, 2013; Harnik et al., 2014). In the Southern

35   Hemisphere (SH), the austral summertime circumpolar jet is located around 40-50 °S, collocated with regions of enhanced surface baroclinicity (e.g., Nakamura and Shimpo, 2004; Koch et al., 2006). During austral winter, a single jet is seen in the Indian Ocean sector, while two distinct branches emerge in the Pacific sector: a subtropical jet at around 30 °S and a polar-front jet at around 60 °S (e.g., Nakamura and Shimpo, 2004; Gallego et al., 2005; Koch et al., 2006). At upper levels, the strongest flow is seen for the Pacific subtropical jet, while at lower levels the flow over the Indian Ocean sector is strongest (e.g., Nakamura and

40   Shimpo, 2004, see also Fig. 1). While the climatological picture shows two distinct jets co-existing in the Pacific sector, these are not well-separated every year (Bals-Elsholz et al., 2001; Nakamura and Shimpo, 2004). On shorter time scales (e.g. days or weeks), we further expect periods when the two jets are merged and others when they are distinct.

The different locations and drivers of the two jet structures, plus the intermediate "merged" jet, issue from very different underlying mechanisms. They in turn result in very different flow characteristics, for example in terms of the jet's variability

45   properties, the wave spectrum and the degree of nonlinearity (e.g., Lachmy and Harnik, 2016, 2019). However, our understanding of the dynamical maintenance mechanisms mostly relies on conceptual or idealised models (e.g., Held and Larichev, 1996; Son and Lee, 2005; Lachmy and Harnik, 2016; Faranda et al., 2019c). Linking these to the phenomena observed in the real atmosphere is therefore key to further our understanding of this major component of the climate system. Our goal in the present study is precisely to provide a concise quantitative overview of the jet characteristics in an idealised atmospheric model

50   and relate them to the large-scale flows in the real atmosphere, as reproduced by reanalysis products. We specifically focus on developing a unitary analysis framework which may be applied to both the idealised model and reanalysis data, and allow for direct intercomparison.

Earth System
Dynamics
Discussions

An idealised model fit for the task at hand should be able to maintain three distinct jet structures: a thermally-driven sub-tropical jet, an eddy-driven polar-front jet and a merged jet. Just as in the real atmosphere, these regimes should differ in the

55 location and variability of the jet stream, as well as in the structure, zonal wavenumber and phase speed of the dominant modes. Here, we use the two-layer modified quasi-geostrophic (QG) spherical model of Lachmy and Harnik (2014). Unlike other QG models, our setup includes advection of the zonal mean momentum by the ageostrophic mean meridional circulation. This enables the model to resolve the momentum balance of the subtropical jet. The model can therefore reproduce the three different jet regimes and their distinct wave–mean flow feedback mechanisms (Lachmy and Harnik, 2016).

60 To elucidate the intrinsic dynamical characteristics of the different regimes, we interpret atmospheric flows as representative of the evolution of chaotic atmospheric attractors. Recent advances in dynamical systems theory have demonstrated that any instantaneous state of a chaotic system may be described by two metrics: the local dimension — related to the system's active degrees of freedom around that particular state — and a local measure of persistence (Lucarini et al., 2016; Faranda et al., 2017b). This approach can easily be applied to a variety of datasets, including reanalysis data, and is thus ideally suited to

65 provide a direct analogy between modelled and observed flows.

The connection between the dynamical systems characteristics of the flow and the jet regimes issues from the wave spectrum and its interaction with the zonal mean flow. According to Lachmy and Harnik (2016), the flow in the idealized two-layer modified QG model transitions from a subtropical jet regime to a merged jet regime and then to an eddy-driven jet regime as the eddy energy is increased. At the transition between the merged and eddy-driven jet regimes, the wave energy spectrum

70 becomes turbulent and an inverse energy cascade takes place. At this transition, an increase in the jet's latitudinal variability and a decrease in its characteristic variability time scale are also seen (Lachmy and Harnik, 2019). We expect these changes to be reflected in the dynamical systems metrics, which reflect the active degrees of freedom and the persistence of the flow.

We first provide a brief overview of the data, model and analysis approaches in Section 2. Sections 3 and 4 outline the dynamical characteristics of the different flow regimes in the model and reanalysis, respectively. Finally, we discuss these

75 results in the context of both idealised models and studies of the observed atmospheric jet, and draw our conclusions in Section 5.

2   Model, Data and Analysis Tools

2.1   The Quasi-Geostrophic Model

The study uses the numerical model of Lachmy and Harnik (2014), designed as a minimal complexity representation of jet

80 dynamics. The model includes the interactions between the zonal mean zonal wind, the mean meridional circulation and the eddies, quantified as deviations from zonal mean values. To balance the heat and momentum budgets, radiative damping to an equilibrium profile and surface friction are also included. The model has two vertical layers, which are meant to represent the lower and upper troposphere. Here, we refer to these with the subscripts l and u, respectively. Two key aspects of the model are: a numerical hyperdiffusion scheme which dissipates energy away from the smallest scales and a representation of the advection

85 of zonal mean momentum by the mean meridional circulation through an ageostrophic term. The waves are treated separately

from the zonal mean flow to allow for a clear conceptual separation between them. This modified QG framework allows the study of the complex interactions between the mean flow, the waves, and the mean meridional circulation, while retaining the simplicity of an idealised model. For a detailed description of the model equations, we refer the reader to Appendix A in Lachmy and Harnik (2014). The main limitations of this setup are discussed in Lachmy and Harnik (2016).

90   The model setup, radiative equilibrium profile, and fixed parameter values used here are the same as in Lachmy and Harnik (2016). These are meant to mimic wintertime conditions. We focus our analysis, both in the model and in the reanalysis data (Sect. 2.2), on the SH because it is closer to zonal symmetry than its northern counterpart. In the model, the different flow regimes are obtained through different combinations of the layer thickness (H) and the wave-damping (r) parameters. r specifically represents the ratio between the damping parameters for the eddies and for the zonal-mean flow. We consider a

95   parameter sweep of 27 different combinations of $7\,km \leq H \leq 10\,km$ and $0.5 \leq r \leq 2$. The numbering of these runs is shown in Table A1.

In the model, we diagnose jet characteristics using: barotropic zonal-mean zonal wind ($0.5 \times (\overline{U_l} + \overline{U_u})$), where overbars denote zonal means) and barotropic wave vorticity ($0.5 \times (q_l + q_u)$). The two give complementary information on the flow, by considering the zonal-mean and the wave fields, respectively. The analysis was repeated using the 3-D (upper and lower

100   levels) full potential vorticity and wave potential vorticity fields, and the results were qualitatively and quantitatively similar (not shown).

2.2   Reanalysis Data

Part of the analysis is conducted on data from the European Centre for Medium-Range Weather Forecasts' ERA-Interim reanalysis (Dee et al., 2011). We use daily average winds interpolated at a horizontal resolution of $0.5\,°$ over the austral winters

105   (June, July and August, JJA) of 1979-2017. We focus on a South Pacific domain spanning $120\,°W - 120\,°E$, $15\,°S - 75\,°S$ (see Fig. 1). This is chosen based on Bals-Elsholz et al. (2001); Nakamura and Shimpo (2004) and Koch et al. (2006) to focus on a longitudinal region with coherent jet characteristics and displaying a range of jet regimes (see also Sect. 4). The jet is diagnosed using the 300 hPa and 850 hPa zonal wind. In analogy with the QG model we take these as representative of upper and lower-level flows. The dynamical systems metric (Sect. 2.3 below) are then computed on barotropic zonal wind, defined

110   as the average of the zonal wind at these two levels. To better compare reanalysis with model results, we further calculate eddy kinetic energy (EKE) from daily data using a six-day high-pass Lanczos filter with 61 weights. EKE indeed provides a clear separation between model jet regimes (Fig. 2a) and can be used to characterise SH jet variability (e.g. Inatsu and Hoskins (2004); Shiogama et al. (2004)).

2.3   Dynamical Systems Metrics

115   The above data is analysed by applying a recently developed approach grounded in dynamical systems theory. This allows computing the instantaneous (in time) or local (in phase-space) properties of a dynamical system by combining extreme value theory with Poincaré recurrences (Lucarini et al., 2016; Faranda et al., 2017b). A given succession of latitude-longitude maps of an atmospheric variable of interest is interpreted as a long trajectory in a reduced phase-space of the atmospheric flow. Each

map corresponds to both a specific point in this phase-space and a specific time. Instantaneity in time is therefore equivalent

120 to locality in phase space. Local (instantaneous) properties are then computed for all points (timesteps) in our dataset. We specifically compute two metrics, namely the local dimension d and the persistence θ^{-1}.

To estimate the local dimension we leverage the Freitas-Freitas-Todd theorem (Freitas et al., 2010), modified by Lucarini et al. (2012), which characterises the system's recurrences around the state of interest ζ. d is a proxy for the number of active degrees of freedom of the system about ζ, and can also be related to the state's intrinsic predictability (Messori et al., 2017;

125 Hochman et al., 2019a). Intuitively, a state with a low local dimension will afford a better predictability than one with a higher d.

The persistence θ^{-1} of a state ζ is a measure of the trajectory's typical residence time in the neighbourhood of ζ. It is obtained from the extremal index, which we compute here using the Süveges estimator (Süveges, 2007). The persistence is bounded in $[1, \infty]$ and is in units of the time step of the data. It is therefore essential to use a dataset whose time step is smaller than the

130 typical timescale of the physical processes of interest. An overly long time step would indeed result in all instantaneous states tending to $\theta^{-1} = 1$. In our case, we deem daily data sufficient to capture the salient features of the large-scale jet variability. Intuitively, highly persistent states should be more predictable than transient ones. Thus, much like d, we may relate θ^{-1} to the system's intrinsic predictability around the state of interest ζ. The fact that both d and θ^{-1} are local metrics implies that this intrinsic predictability is conceptually different from the predictability inferred from the performance of a numerical weather

135 prediction model. The two are, however, partly related (Scher and Messori, 2018).

As final product, one obtains a value of d and θ^{-1} for every time step and variable in the dataset. This approach has been successfully tested on a variety of climate datasets (e.g., Faranda et al., 2017a; Rodrigues et al., 2018; Scher and Messori, 2019; Hochman et al., 2019a, b; De Luca et al., 2019; Faranda et al., 2020), and is more generally applicable to a broad range of chaotic dynamical systems. For a detailed derivation of d and θ^{-1}, we refer the reader to Lucarini et al. (2016) and Faranda

140 et al. (2019a, b).

3 Dynamical system characteristic of jet regimes in a 2-layer QG model

3.1 Model jet regimes

The simple model we adopt can reproduce the three jet regimes: subtropical, merged and eddy-driven. We classify our simulations following Lachmy and Harnik (2016). As the wave energy is increased by decreasing H and/or r (Sect. 2.1), the flow

145 transitions from a subtropical jet regime to a merged jet regime and finally to an eddy-driven jet regime (Fig. 2a). The three regimes are characterized by different zonal-mean zonal wind structures (Fig. A1), driving mechanisms, and eddy spectral properties (Fig. 2b). The subtropical jet is located at the edge of the Hadley cell, and is maintained by zonal-mean advection of planetary momentum. The merged jet is located inside the Ferrel cell and is maintained by eddy momentum flux convergence from a wavenumber 5-dominated spectrum. It has a narrow latitudinal structure and very weak latitudinal variability. The eddy-

150 driven jet is wider and displays large fluctuations. The eddy momentum flux convergence which maintains it is associated with a wide wave spectrum (Fig. 2b). The model further reproduces flows which are a mixture of the eddy-driven and merged jet

regimes, meaning that the simulations either vacillate between the two regimes or that the flow displays characteristics of both regimes, depending on the chosen diagnostic variable (crosses in Fig. 2, Lachmy and Harnik (2016)). The characterization of the different flow regimes is detailed in Appendix A.

3.2 Dynamical characteristics of the model jet regimes

The three jet regimes (plus the mixed case) reproduced by the model display very different temporal variability (Sect. 3.1, Lachmy and Harnik, 2019), suggesting that their dynamical systems characteristics should be well-separated. Specifically, wave driving is the dominant mechanism affecting the jet and its variability on a wide range of time scales. A strong EKE should favour nonlinearities in the flow and allows for a rich set of possible evolutions. The converse holds for weak EKE. We would thus expect the jet stream to be more persistent (smaller θ) and display a lower local dimension d when the EKE is weak.

We analyse the results for d and θ computed on both barotropic zonal mean zonal wind and barotropic wave vorticity (Fig. 3). The former (Fig. 3b, d) displays increasing d and θ as the flow transitions from the weak EKE subtropical jet regime (red dots), to the mid-range EKE merged jet (green dots), to the strong EKE eddy-driven jet regimes (black dots), via the mixed cases (blue dots). Although all regimes display a large internal variability, the (d, θ) centroids for each simulation highlight a clear dynamical separation (Fig. 3d).

The picture from the barotropic wave vorticity is more nuanced (Fig. 3a, c). The subtropical jet regime (red dots) typically displays low d and θ, matching the expected weak wave activity and the dominance of thermal maintaining mechanisms. The eddy-driven jet regime shows a higher d and θ, reflecting the dominant role of eddies and the large meridional excursions in jet location (black dots). The merged jet regime (green dots) and mixed cases (blue dots) display lower d than the eddy-driven jet regime, yet a higher θ. This is a somewhat unusual combination, both in terms of our *a priori* expectations on the dynamical characteristics of the different jet regimes and in terms of the positive correlation between d and θ displayed by most atmospheric variables (e.g., Faranda et al., 2017b, a; Messori et al., 2017). This result may reflect the narrow wave spectrum driving the merged jet regime, leading to a quasi-periodic behaviour. The regime is therefore persistent – in the sense of having a low windspeed variability and weak meridional meandering of the jet – but does not emerge as such in the θ metric due to the specificity of its wave spectrum. The fact that for the barotropic zonal mean zonal wind (Fig. 3b, d) the d and θ of the merged jet regime lie in-between the subtropical and eddy-driven jet regimes, strengthens our interpretation of the unusual parameter combination for the barotropic wave vorticity of former regime as issuing from the peculiarity of its wave spectrum.

A more detailed picture of the evolution of the flow's dynamical characteristics can be obtained by ranking the different simulations by decreasing EKE, which closely mirrors the division between the different jet regimes (Fig. 4). The barotropic wave vorticity displays an increase in θ at the transition between the eddy driven and merged jet regimes, and a large discontinuous decrease in θ at the transition between the merged and subtropical jet regimes around simulation 23 (Fig. 4a). The latter simulation is discussed in further detail below. The large values of θ in the merged jet regime, which indicate low persistence, are likely due to the latter's narrow wave spectrum discussed above (see also Fig. 2b). The barotropic wave vorticity d shows instead a decrease as a function of EKE, albeit with significant variability within the individual jet regimes. The highest val-

Earth System
Dynamics
Discussions

ues of d appear in the most energetic simulations of the eddy driven-jet regime, consistent with their turbulent nature as seen in the wave spectrum (Fig. 2b) and also discussed in Lachmy and Harnik (2016). Both dynamical metrics for the barotropic zonal mean zonal wind (Fig. 4b, d) display a largely monotonic decrease with increasing simulation index. Again, the transitions between different jet regimes, and especially that between the merged and subtropical jet regimes (around simulation

190   23), emerge as discontinuities. Fig. 4 also highlights the range of variability of the dynamical systems metrics within each simulation. Some distributions, such as the local dimension of the subtropical jet regime (Fig. 4c), are very peaked, indicating homogeneous characteristics of the flow throughout the simulations. Others, such as the eddy-driven regime in the same panel, display a broader peak and a wider range of variability, pointing to the rich dynamical structure of the flow.

We conclude the overview of the QG model's jet regimes by focusing on simulation no. 23, which serves well to illustrate

195   the sensitivity of the dynamical systems metrics to the instantaneous characteristics of the atmospheric flow. This simulation falls within the subtropical jet regime (Table A1 and Fig. 2a), but displays some anomalous characteristics. These are clearly visible in Fig. 4, but also emerge in Fig. 3a as a cloud of red points extending towards high θ values. Simulation no. 23 mostly fits the characteristics of a subtropical jet regime, but displays anomalous characteristics for a period of approximately 1200 days in the middle of the simulation (Fig. 5c). This is characterised by vacillations between a high-EKE, southerly merged

200   jet regime and a subtropical jet. Unlike the mixed jet simulations, however, this is an isolated occurrence, explaining why the simulation falls into the subtropical jet classification. The dynamical systems metrics identify clearly this anomalous transition period (red dots in Fig. 5a, b), which covers a separate region of the d–θ space compared to the rest of the simulation. Indeed, the outcropping region in Fig. 3a can be almost exclusively ascribed to the anomalous period (cf. Figs. 3a, 5a). The barotropic wave vorticity of this period is intermediate between the merged jet and subtropical jet clusters (red cross in Fig. 3c), while the

205   barotropic zonal mean zonal wind displays anomalously low local dimension and persistence (red crosses in Fig. 3d, Fig. 3b).

4   Dynamical characteristics of jet regimes in reanalysis data

As discussed in the introduction, pure thermally-driven or eddy-driven jets are largely theoretical constructs. Moreover, for a given region and season, the jet typically displays large intraseasonal variability and a range of different flow characteristics (e.g., Bals-Elsholz et al., 2001; Nakamura and Shimpo, 2004; Woollings et al., 2010; Harnik et al., 2014; Messori and Caballero,

210   2015; Madonna et al., 2017). On these bases, we expect the jets observed in the real atmosphere to blend the dynamical characteristics of the different jet regimes reproduced in the QG model.

To verify whether our dynamical systems approach can distinguish between different jet regimes in the real atmosphere, we therefore take a slightly different angle from that used in our idealised model, although the analysis tools are identical to those used above. We compute d and θ on barotropic zonal wind (see Sect. 2.2), but consider flow anomalies associated with

215   concurrent low or high values of d and θ. We define these as values beyond the 10th or 90th percentiles of the respective distributions. This choice is dictated by the clear separation of regimes along a d–θ diagonal in Fig. 3. The analysis focuses on the JJA months over the Pacific domain shown in Fig. 1, chosen because it displays a variety of jet regimes. During the Austral winter, the signature of the subtropical – and predominantly thermally-driven – jet is evident at upper levels around

Earth System
Dynamics
Discussions

30 °S, while that of the polar – and predominantly eddy-driven – jet emerges most clearly at lower levels around 60 °S (Fig.
220 1). Periods when these flows are well-separated alternate with periods dominated by a single near-barotropic flow, akin to a
merged jet.

When both d and θ are anomalously low, the upper-level zonal wind (300 hPa) displays a clear maximum around 30 °S,
coincident with the climatological location of the subtropical jet and characterised by above-average speeds (Fig. 6a). The
signature of this jet extends to the lower troposphere, where a low-level (850 hPa) zonal wind maximum located slightly
225 poleward of the 300 hPa maximum, is clearly visible on the same days, especially in the eastern part of the domain (Fig. 6c).
This inference is confirmed by analysing the vertical cross-section of the zonal flow, which evidences a poleward displacement
of the location of the zonal wind maximum at 850 hPa compared to 300 hPa (Fig. 7a). The EKE shows widespread negative
anomalies across the central and southern portions of the domain, and localised positive anomalies at 300 hPa matching the
latitude of the jet (Fig. 8a, c). We interpret the above characteristics as the signature of a merged jet.

230 When both d and θ are anomalously high, the upper-level zonal flow evidences two maxima: a weaker-than-climatology jet
around 30 °S and an anomalous secondary maximum at around 55 °S, associated with large positive zonal windspeed anomalies
(Fig. 6b). At low levels, there is a single jet located just to the North of 60 °S and associated with large positive zonal flow
anomalies (Fig. 6d). The southern jet therefore has a more pronounced barotropic structure than its northern counterpart, as
also seen in the vertical cross-section of the zonal flow (Fig. 7b). The EKE anomalies are predominantly positive across the
235 central and southern portions of the domain (Fig. 8b, d). The above points to a primarily eddy-driven jet in the South and a
primarily thermally-driven jet further North, in agreement with the theoretical framework of Lee and Kim (2003) and Son and
Lee (2005). It also suggests that the persistence of the double-jet configuration, with a strong eddy-driven jet, is lower (high θ)
than that of the single, predominantly thermally-driven jet (low θ).

5 Discussion and conclusions

240 We have analysed different jet regimes in a set of idealised simulations with a QG model and reanalysis data. The QG model
reproduces the full range of theoretically-derived jet regimes (e.g., Lee and Kim, 2003; Son and Lee, 2005; Lachmy and Harnik,
2016). These are: an eddy-driven jet, a merged jet and a subtropical jet. It additionally reproduces transition states between
a merged and eddy-driven jet, which we term mixed jets. Pure eddy-driven or thermally-driven jets are largely theoretical
constructs, and in the real atmosphere the separation between them is often blurred. Nonetheless, it is possible to identify
245 primarily eddy-driven, primarily thermally-driven and merged jets (e.g., Koch et al., 2006; Eichelberger and Hartmann, 2007;
Li and Wettstein, 2012). The South Pacific sector is of particular interest in this context, since it is a region where the three
main jet regimes may be observed at the same longitude (e.g., Bals-Elsholz et al., 2001; Nakamura and Shimpo, 2004).

Relating the different jet regimes identified in idealised models to those identified in reanalysis data is far from immediate.
Here, we have proposed an analysis approach which may be applied to both datasets, and which provides a direct link between
250 the characteristics of the jets in the QG model and those seen in the ERA-Interim dataset. Such approach is grounded in
dynamical systems theory and is based on two metrics, d and θ, which characterise the instantaneous (local in phase-space)

Earth System
Dynamics
Discussions

Open Access

EGU

dynamical characteristics of the jet. The local dimension d is a proxy for the number of active degrees of freedom of the system. The persistence θ^{-1} is a measure of the typical residence time of the system in the neighbourhood of a given state. Their computation issues from an analysis of recurrences of the system, and both may be intuitively related to the concept

255   of predictability. Indeed, one main expect low d, high θ^{-1} states to be more predictable than high d low θ^{-1} situations. Unlike conventional approaches which diagnose the driving mechanisms of the jet in terms of complex physical processes, such as convection or eddy momentum flux convergence, here we infer the dynamical properties of the system uniquely from computing d and θ on the wind itself. As a caveat, we note that the absolute values of these metrics should be interpreted in a relative sense within each dataset they are computed on, and that direct comparison of their magnitudes across datasets

260   should be treated with caution. From a theoretical standpoint, there are cogent arguments supporting the use of recurrences of observables of a system to investigate the properties of the system's underlying phase-space, even though all the variables defining said phase-space cannot be considered (e.g., Faranda et al., 2017a, c; Barros et al., 2019). This makes our analysis unexpensive in terms of computational and data requirements, and versatile in terms of applicability to very different datasets. Moreover, d and θ do not require prior knowledge of the exact location of the jet.

265   In the QG model, d and θ successfully distinguish between the different jet regimes. Specifically, when computed on barotropic zonal mean zonal wind they highlight the purely eddy-driven jet as being a low-persistence, high dimensional regime, the purely thermally-driven jet as being a high-persistence, low dimensional regime and the merged jet as having inter-mediate dynamical characteristics. This reflects theoretical expectations on the role of increased EKE on predictability (Leith, 1971). The results for reanalysis largely mirror those found for the idealised simulations. Focusing on the Pacific sector of the

270   Southern Ocean, d and θ computed on the barotropic zonal wind again discriminate between different jet regimes. Specifically, high d, high θ days display both a thermally-driven, subtropical jet and a strong eddy-driven, polar-front jet, while low d, low θ days display a merged jet. The key difference between the two analyses is that, in the reanalysis data, we do not observe a single subtropical nor a single eddy-driven jet.

Our intention is not to provide a systematic analysis of atmospheric jet characteristics in different geographical regions.
275   Rather, by building upon both idealised simulations and reanalysis data, we provide a proof-of-concept for using dynamical systems indicators to diagnose jet regimes in a versatile and conceptually intuitive fashion.

Appendix A: Definition of the jet regimes in the 2-layer QG model

The flow regimes in the 2-layer QG model, described in section 2.1, are characterized according to the structure of the zonal-mean flow and the properties of the wave spectrum, following Lachmy and Harnik (2016). The diagnosed regimes for each of

280   the simulations are listed in Table A1.

The different structures of the zonal-mean zonal wind are shown in Fig. A1 for three simulations, one from each regime. The upper layer zonal wind (thick solid lines) represents the upper tropospheric jet stream. The lower layer zonal wind (thin dashed lines) indicates the structure of the mean meridional circulation, since according to the zonal-mean momentum balance, it is positive in the Ferrel cell and negative in the Hadley and polar cells (Lachmy and Harnik, 2014). We identify the mechanism

285   maintaining the jet according to the relative location of the upper and lower layer zonal wind maxima. The subtropical jet
(black lines) is thermally driven, since its upper-layer zonal wind maximum is at the Hadley cell edge, where the lower layer
zonal wind is zero. The merged jet (red lines) and eddy-driven jet (blue lines) are located inside the Ferrel cell, where the lower
layer zonal wind is maximal, indicating that they are driven by eddy momentum flux convergence. In the merged jet regime
the jet inside the Ferrel cell is collocated with the maximal vertical shear of the zonal wind, which indicates that it represents
290   a merging of the subtropical and eddy-driven jets. In the eddy-driven jet regime the two maxima are separated, indicating that
the upper layer zonal wind maximum represents a purely eddy-driven jet (Lachmy and Harnik, 2016).

Code availability. The code to compute the dynamical systems metrics is freely available from: https://www.lsce.ipsl.fr/Phocea/file.php?
class=pisp&reload=1511429128&file=davide.faranda/files/249/dimensione_faranda_NCEP.R

Author contributions. G. Messori and N. Harnik designed the study. N. Harnik and O. Lachmy performed the analysis of the jet regimes on
295   model data. D. Faranda performed the dynamical systems analysis on model data. E. Madonna and G. Messori performed the analysis on
ERA-Interim data. All authors contributed to drafting the manuscript.

Competing interests. The authors declare that they have no competing interests

References

300 Bals-Elsholz, T. M., Atallah, E. H., Bosart, L. F., Wasula, T. A., Cempa, M. J., and Lupo, A. R.: The wintertime Southern Hemisphere split jet: Structure, variability, and evolution, Journal of climate, 14, 4191–4215, 2001.

Barros, V., Liao, L., and Rousseau, J.: On the shortest distance between orbits and the longest common substring problem, Advances in Mathematics, 344, 311–339, 2019.

De Luca, P., Messori, G., Pons, F., and Faranda, D.: Dynamical Systems Theory Sheds New Light on Compound Climate Extremes in Europe

305 and Eastern North America, Quarterly Journal of the Royal Meteorological Society, 2019.

Dee, D. P., Uppala, S., Simmons, A., Berrisford, P., Poli, P., Kobayashi, S., Andrae, U., Balmaseda, M., Balsamo, G., Bauer, d. P., et al.: The ERA-Interim reanalysis: Configuration and performance of the data assimilation system, Quarterly Journal of the royal meteorological society, 137, 553–597, 2011.

Eichelberger, S. J. and Hartmann, D. L.: Zonal jet structure and the leading mode of variability, Journal of Climate, 20, 5149–5163, 2007.

310 Faranda, D., Messori, G., Alvarez-Castro, M. C., and Yiou, P.: Dynamical properties and extremes of Northern Hemisphere climate fields over the past 60 years, Nonlinear Processes in Geophysics, 24, 713–725, 2017a.

Faranda, D., Messori, G., and Yiou, P.: Dynamical proxies of North Atlantic predictability and extremes, Scientific reports, 7, 41 278, 2017b.

Faranda, D., Sato, Y., Saint-Michel, B., Wiertel, C., Padilla, V., Dubrulle, B., and Daviaud, F.: Stochastic chaos in a turbulent swirling flow, Physical review letters, 119, 014 502, 2017c.

315 Faranda, D., Alvarez-Castro, M. C., Messori, G., Rodrigues, D., and Yiou, P.: The hammam effect or how a warm ocean enhances large scale atmospheric predictability, Nature communications, 10, 1316, 2019a.

Faranda, D., Messori, G., and Vannitsem, S.: Attractor dimension of time-averaged climate observables: insights from a low-order ocean-atmosphere model, Tellus A: Dynamic Meteorology and Oceanography, 71, 1–11, 2019b.

Faranda, D., Sato, Y., Messori, G., Moloney, N. R., and Yiou, P.: Minimal dynamical systems model of the northern hemisphere jet stream

320 via embedding of climate data, Earth System Dynamics, 10, 555–567, 2019c.

Faranda, D., Messori, G., and Yiou, P.: Diagnosing concurrent drivers of weather extremes: application to warm and cold days in North America, Climate Dynamics, pp. 1–15, 2020.

Freitas, A. C. M., Freitas, J. M., and Todd, M.: Hitting time statistics and extreme value theory, Probability Theory and Related Fields, 147, 675–710, 2010.

325 Gallego, D., Ribera, P., Garcia-Herrera, R., Hernandez, E., and Gimeno, L.: A new look for the Southern Hemisphere jet stream, Climate Dynamics, 24, 607–621, 2005.

Harnik, N., Galanti, E., Martius, O., and Adam, O.: The anomalous merging of the African and North Atlantic jet streams during the Northern Hemisphere winter of 2010, Journal of Climate, 27, 7319–7334, 2014.

Heaviside, C. and Czaja, A.: Deconstructing the Hadley cell heat transport, Quarterly Journal of the Royal Meteorological Society, 139,

330 2181–2189, 2013.

Held, I. M.: Momentum transport by quasi-geostrophic eddies, Journal of the Atmospheric Sciences, 32, 1494–1497, 1975.

Held, I. M. and Hou, A. Y.: Nonlinear axially symmetric circulations in a nearly inviscid atmosphere, Journal of the Atmospheric Sciences, 37, 515–533, 1980.

Held, I. M. and Larichev, V. D.: A scaling theory for horizontally homogeneous, baroclinically unstable flow on a beta plane, Journal of the

335 Atmospheric Sciences, 53, 946–952, 1996.

Earth System
Dynamics
Discussions
EGU
Open Access

Hochman, A., Alpert, P., Harpaz, T., Saaroni, H., and Messori, G.: A new dynamical systems perspective on atmospheric predictability: Eastern Mediterranean weather regimes as a case study, Science advances, 5, eaau0936, 2019a.

Hochman, A., Alpert, P., Kunin, P., Rostkier-Edelstein, D., Harpaz, T., Saaroni, H., and Messori, G.: The dynamics of cyclones in the twentyfirst century: the Eastern Mediterranean as an example, Climate Dynamics, pp. 1–14, 2019b.

340 Hoskins, B. J., James, I. N., and White, G. H.: The shape, propagation and mean-flow interaction of large-scale weather systems, Journal of the atmospheric sciences, 40, 1595–1612, 1983.

Inatsu, M. and Hoskins, B. J.: The zonal asymmetry of the Southern Hemisphere winter storm track, Journal of climate, 17, 4882–4892, 2004.

Koch, P., Wernli, H., and Davies, H. C.: An event-based jet-stream climatology and typology, International Journal of Climatology: A Journal

345 of the Royal Meteorological Society, 26, 283–301, 2006.

Lachmy, O. and Harnik, N.: The transition to a subtropical jet regime and its maintenance, Journal of the Atmospheric Sciences, 71, 1389–1409, 2014.

Lachmy, O. and Harnik, N.: Wave and jet maintenance in different flow regimes, Journal of the Atmospheric Sciences, 73, 2465–2484, 2016.

Lachmy, O. and Harnik, N.: Tropospheric jet variability in different flow regimes, Quarterly Journal of the Royal Meteorological Society,

350 2019.

Lee, S.: Maintenance of multiple jets in a baroclinic flow, Journal of the atmospheric sciences, 54, 1726–1738, 1997.

Lee, S. and Kim, H.-k.: The dynamical relationship between subtropical and eddy-driven jets, Journal of the atmospheric sciences, 60, 1490–1503, 2003.

Leith, C.: Atmospheric predictability and two-dimensional turbulence, Journal of the Atmospheric Sciences, 28, 145–161, 1971.

355 Li, C. and Wettstein, J. J.: Thermally driven and eddy-driven jet variability in reanalysis, Journal of Climate, 25, 1587–1596, 2012.

Lucarini, V., Faranda, D., and Wouters, J.: Universal behaviour of extreme value statistics for selected observables of dynamical systems, Journal of statistical physics, 147, 63–73, 2012.

Lucarini, V., Faranda, D., de Freitas, J. M. M., Holland, M., Kuna, T., Nicol, M., Todd, M., Vaienti, S., et al.: Extremes and recurrence in dynamical systems, John Wiley & Sons, 2016.

360 Madonna, E., Li, C., Grams, C. M., and Woollings, T.: The link between eddy-driven jet variability and weather regimes in the North Atlantic-European sector, Quarterly Journal of the Royal Meteorological Society, 143, 2960–2972, 2017.

Messori, G. and Caballero, R.: On double Rossby wave breaking in the North Atlantic, Journal of Geophysical Research: Atmospheres, 120, 11–129, 2015.

Messori, G., Caballero, R., and Faranda, D.: A dynamical systems approach to studying midlatitude weather extremes, Geophysical Research

365 Letters, 44, 3346–3354, 2017.

Nakamura, H. and Shimpo, A.: Seasonal variations in the Southern Hemisphere storm tracks and jet streams as revealed in a reanalysis dataset, Journal of Climate, 17, 1828–1844, 2004.

O'Rourke, A. K. and Vallis, G. K.: Jet interaction and the influence of a minimum phase speed bound on the propagation of eddies, Journal of the Atmospheric Sciences, 70, 2614–2628, 2013.

370 Panetta, R. L.: Zonal jets in wide baroclinically unstable regions: Persistence and scale selection, Journal of the atmospheric sciences, 50, 2073–2106, 1993.

Rhines, P. B.: Waves and turbulence on a beta-plane, Journal of Fluid Mechanics, 69, 417–443, 1975.

Earth System
Dynamics
Discussions

Rodrigues, D., Alvarez-Castro, M. C., Messori, G., Yiou, P., Robin, Y., and Faranda, D.: Dynamical properties of the North Atlantic atmospheric circulation in the past 150 years in CMIP5 models and the 20CRv2c reanalysis, Journal of Climate, 31, 6097–6111, 2018.

375 Scher, S. and Messori, G.: Predicting weather forecast uncertainty with machine learning, Quarterly Journal of the Royal Meteorological Society, 144, 2830–2841, 2018.

Scher, S. and Messori, G.: Weather and climate forecasting with neural networks: using general circulation models (GCMs) with different complexity as a study ground, Geoscientific Model Development, 12, 2797–2809, 2019.

Shiogama, H., Terao, T., and Kida, H.: The role of high-frequency eddy forcing in the maintenance and transition of the Southern Hemisphere
380 annular mode, Journal of the Meteorological Society of Japan. Ser. II, 82, 101–113, 2004.

Son, S.-W. and Lee, S.: The response of westerly jets to thermal driving in a primitive equation model, Journal of the atmospheric sciences, 62, 3741–3757, 2005.

Süveges, M.: Likelihood estimation of the extremal index, Extremes, 10, 41–55, 2007.

Woollings, T., Hannachi, A., and Hoskins, B.: Variability of the North Atlantic eddy-driven jet stream, Quarterly Journal of the Royal
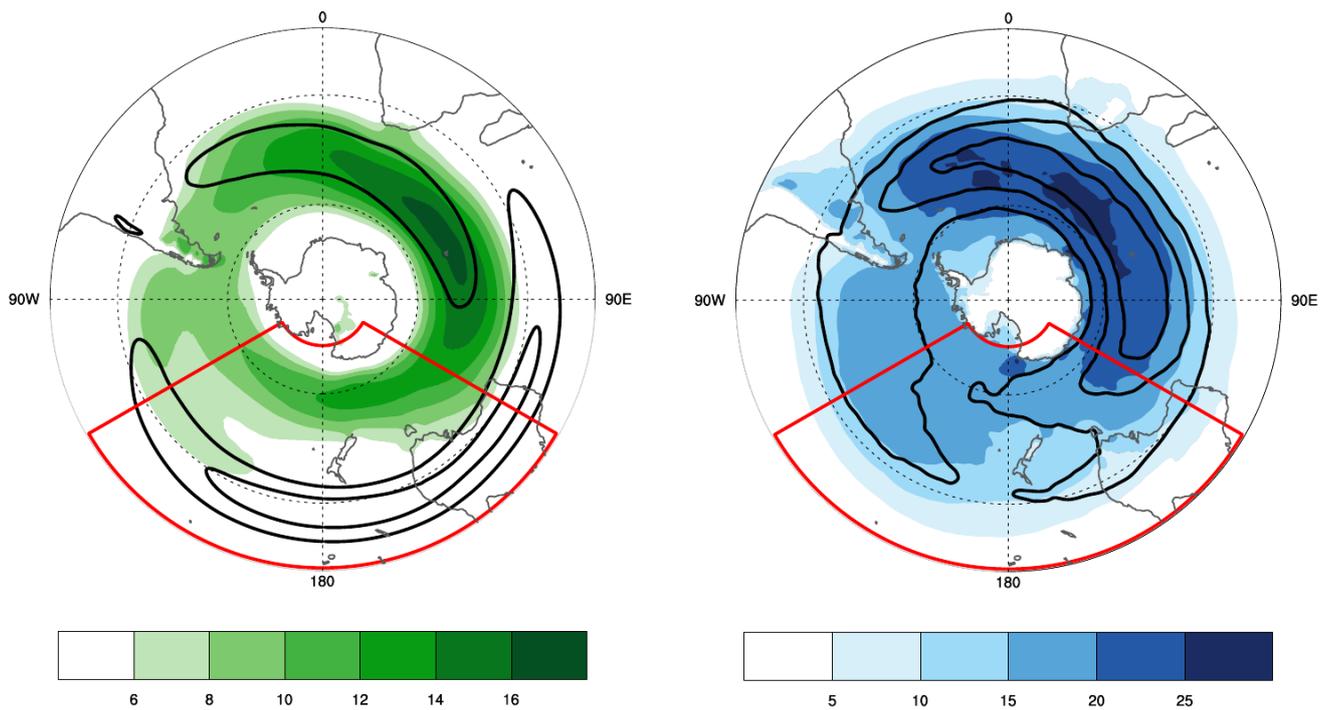385 Meteorological Society, 136, 856–868, 2010.

Figure 1. Climatological JJA zonal wind ($m\ s^{-1}$, a) and eddy kinetic energy (EKE, $m^2\ s^{-2}$, b). Colours show variables on the 850 hPa surface and contours on the 300 hPa surface. Contours are at $30\ m\ s^{-1}$ and $40\ m\ s^{-1}$ in (a), and every $20\ m^2\ s^{-2}$, starting from $60\ m^2\ s^{-2}$, in (b). The red boxes shows the South Pacific domain [$120\,°$W–$120\,°$E, $15\,°$–$75\,°$S]
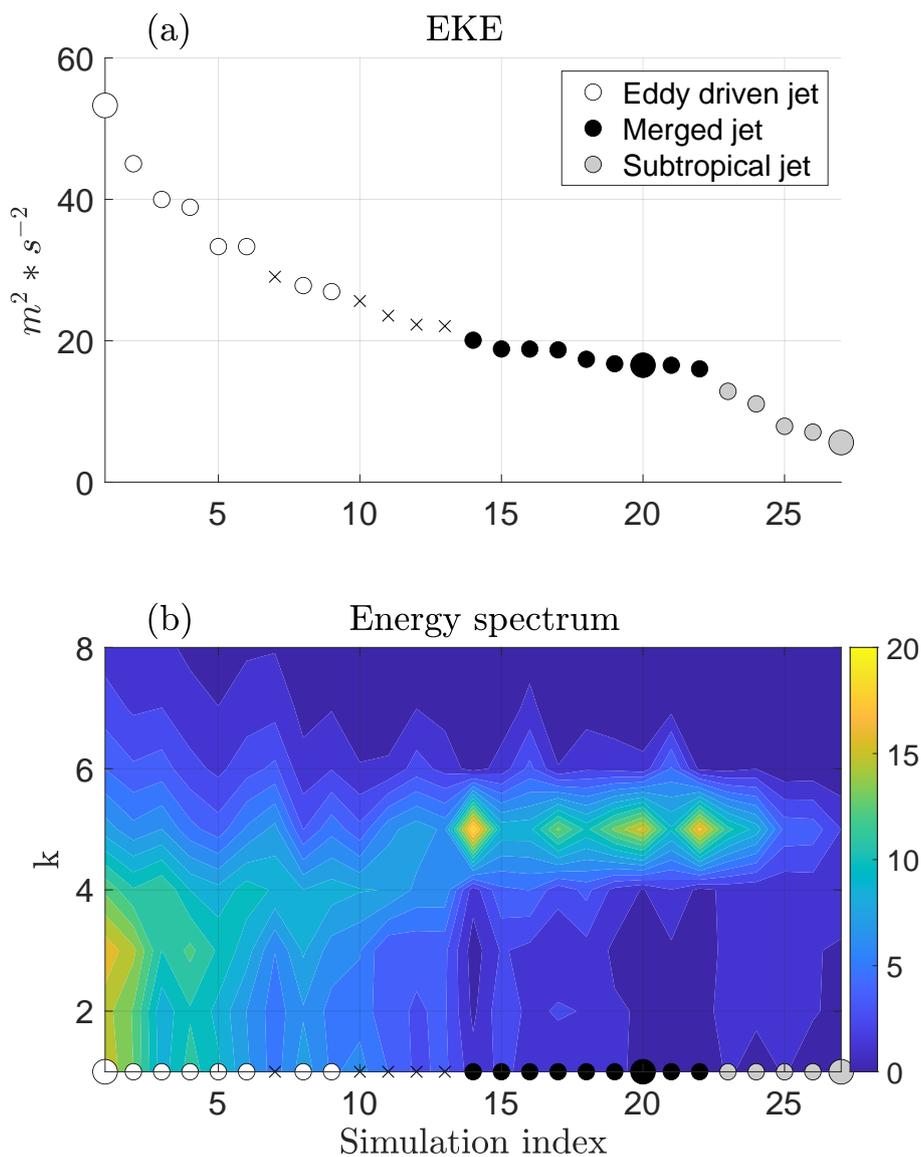
Figure 2. (a) Time-mean eddy kinetic energy (EKE), averaged over the model's Southern Hemisphere and (b) eddy energy spectrum as a function of zonal wavenumber k and simulation index (see Table A1). Units are $m^2\ s^{-2}$ for both panels. The markers on both panels indicate the jet regime of each simulation. Open circles, black circles, gray circles and ×'s indicate eddy-driven jet, merged jet, subtropical jet and mixed (eddy-driven and merged jet) regimes, respectively (see text for the characterization of the jet regimes). The larger markers indicate the simulations shown in Fig. A1.

Figure 3. d–θ diagrams of barotropic wave vorticity (a,c) and barotropic zonal mean zonal wind (b,d) for all timesteps in the simulations (a,b) and centroids for each different model simulation. Colours indicate the different jet regimes. The red + symbols in (c, d) mark the centroids of the anomalous period in simulation no. 23, discussed in Sect. 3.2. Note that the axes' ranges differ across the panels.
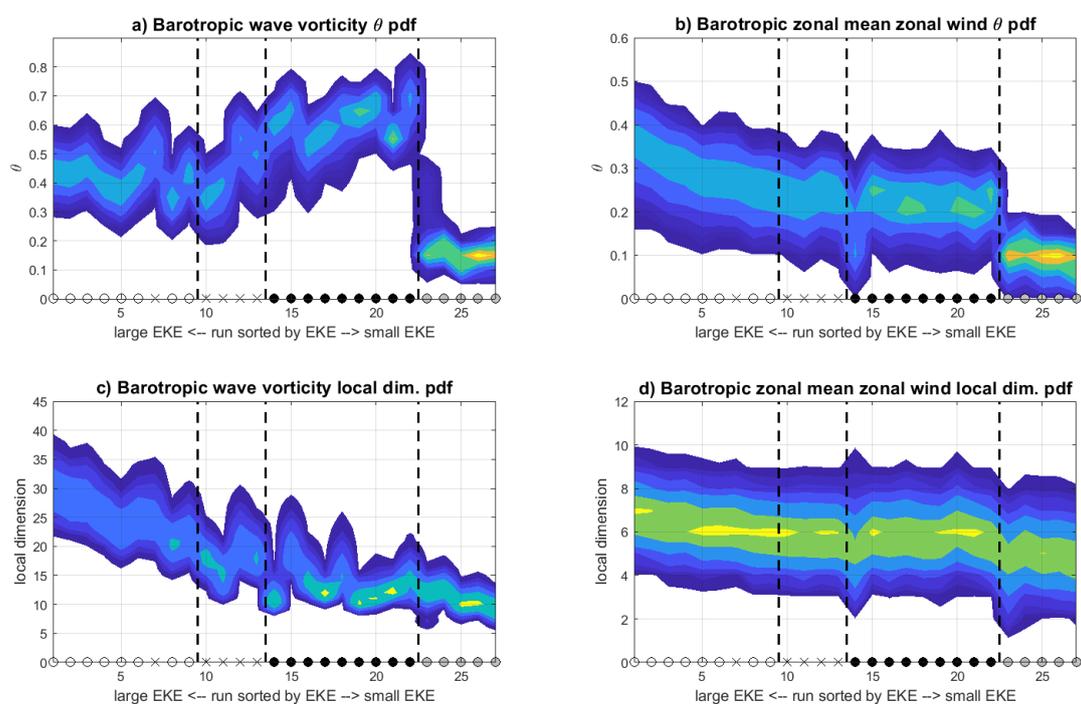
Figure 4. Distributions of θ (a, b) and d (c, d) values for barotropic wave vorticity (a,c) and barotropic zonal mean zonal wind (b,d) in the different model runs. The markers on the x-axis indicate the flow regime, as in Fig. 2. The vertical dashed lines indicate the approximate transitions between the different jet regimes. Note that the ordinates' ranges differ across panels.
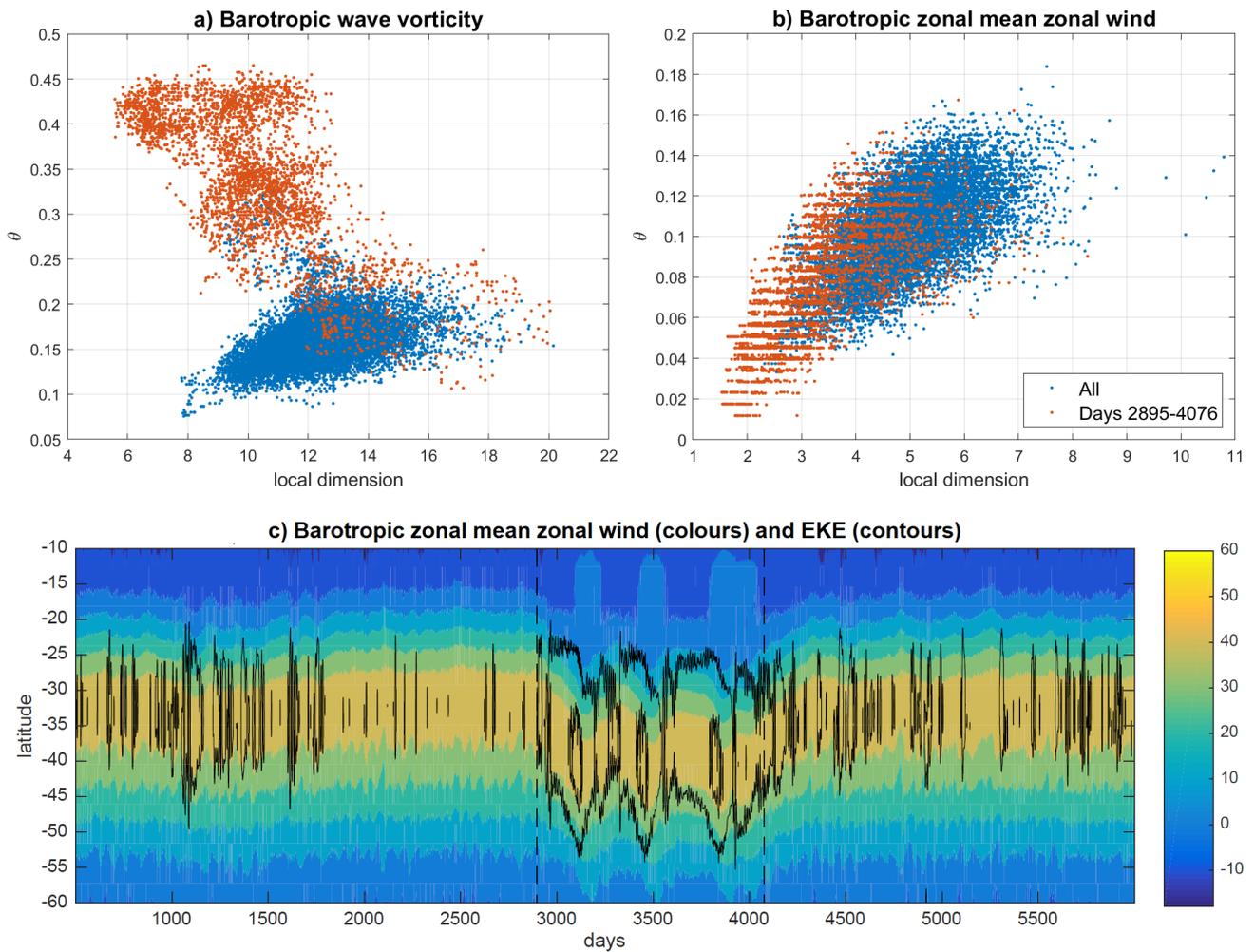
Figure 5. d–θ diagrams of barotropic wave vorticity (a) and barotropic zonal mean zonal wind (b) for all timesteps in simulation no. 23. (c) Latitude – time diagram of barotropic zonal mean zonal wind (colours) and eddy kinetic energy (EKE, contours) for the same simulation. The red dots in (a, c) correspond to days 2895-4076 in the simulation, marked by the two vertical dashed lines in (c).
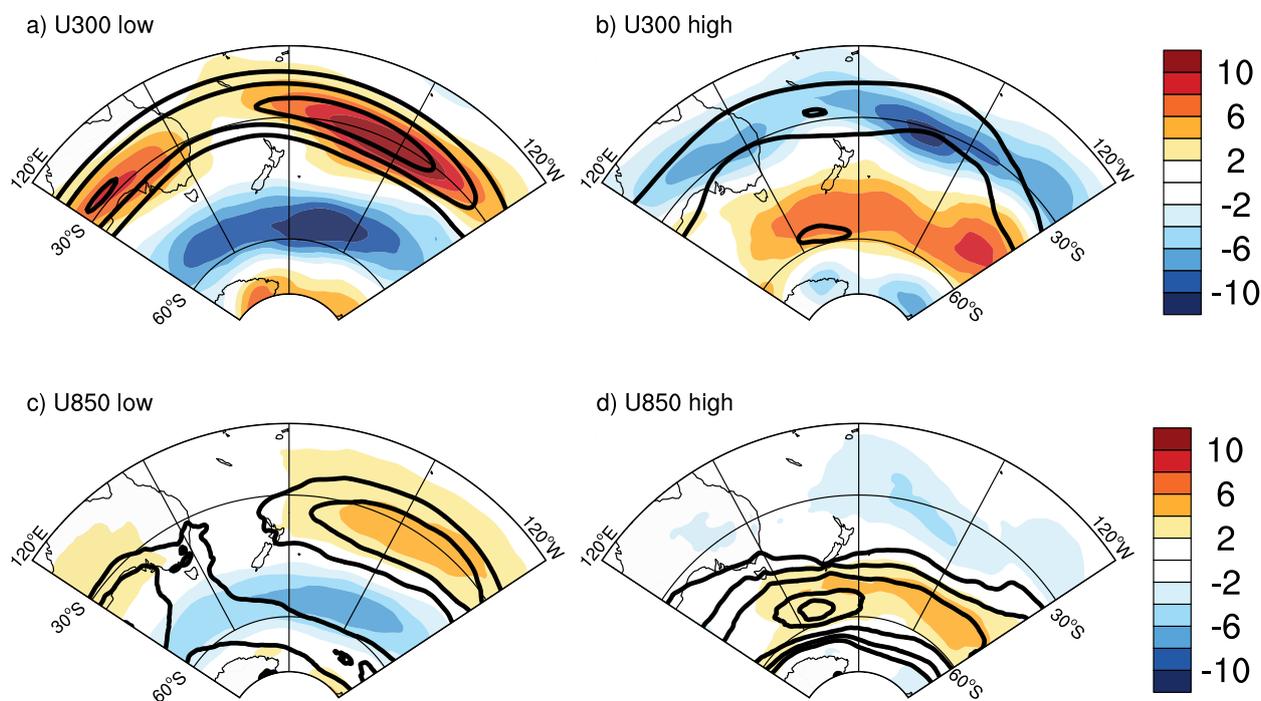
Figure 6. JJA zonal wind composites ($m\ s^{-1}$) at 300 hPa (a, b) and 850 hPa (c, d) for days displaying low (a, c) and high (b, d) values of d and θ. See text for details. Colours show deviations from the climatology, while contours show absolute values. Contours are every 10 m s^{-1}, starting from 30 $m\ s^{-1}$ in (a, b) and every 3 $m\ s^{-1}$, starting from 6 $m\ s^{-1}$ in (c, d).
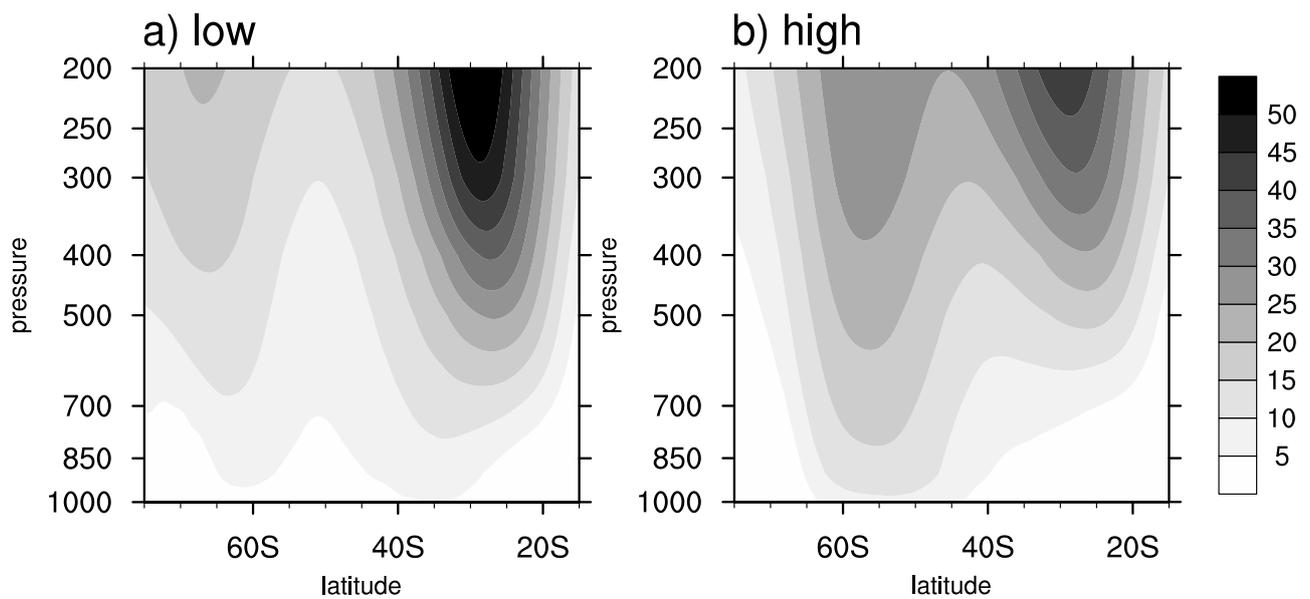
Figure 7. JJA zonal mean zonal wind cross-sections ($m\ s^{-1}$) over the South Pacific domain [120 °W–120 °E], for days displaying low (a) and high (b) values of d and θ. See text for details.
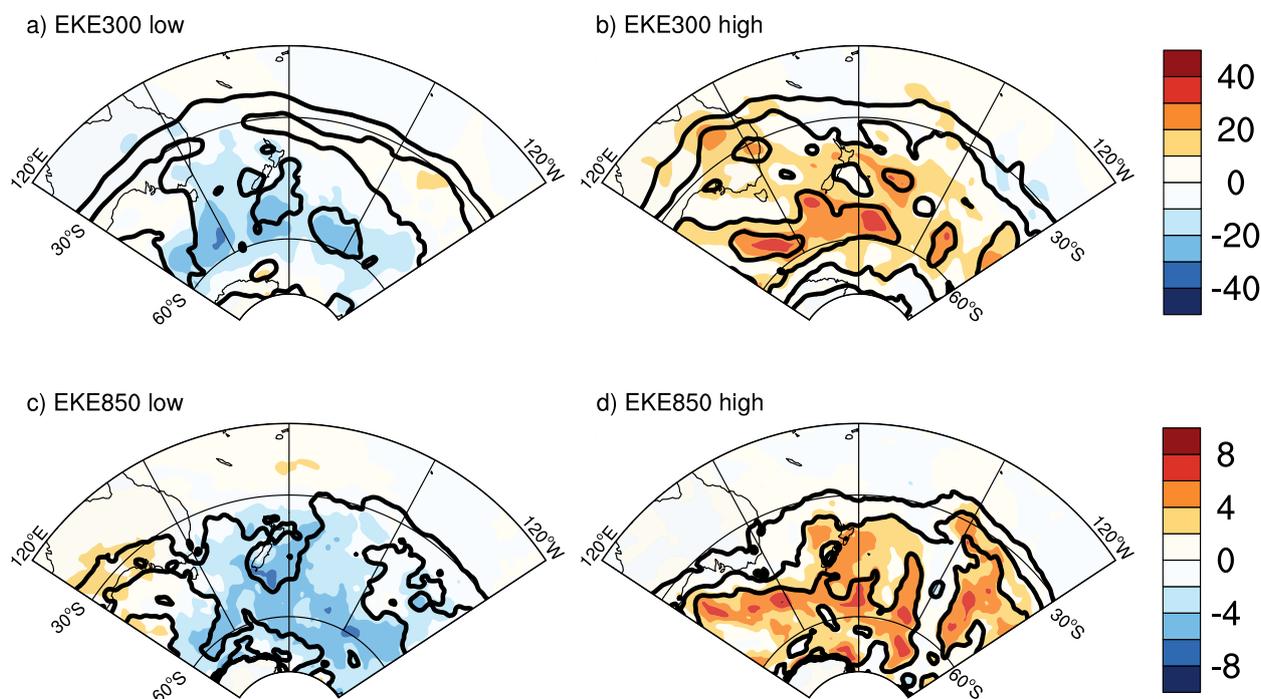
Figure 8. JJA EKE composites ($m^2\ s^{-2}$) at 300 hPa (a, b) and 850 hPa (c, d) for days displaying low (a, c) and high (b, d) values of d and θ. See text for details. Colours show deviations from the climatology, while contours show absolute values. Contours are every 20 $m^2\ s^{-2}$, starting from 40 $m^2\ s^{-2}$ in (a, b) and every 5 $m^2\ s^{-2}$, starting from 10 $m^2\ s^{-2}$ in (c, d).

Earth System
Dynamics

Open Access

Discussions

EGU

Table A1. The model simulations, sorted by the EKE in descending order. The parameters H and r are the layer thickness in km and the dimensionless wave damping parameter, respectively. The simulations are categorized according to their flow regime (see text). Simulations with mixed properties of the merged jet and eddy driven jet regimes are denoted as "mixed properties".

Simulation index	H	r	Flow regime
1	7	0.5	Eddy driven jet
2	7.5	0.5	Eddy driven jet
3	7	1	Eddy driven jet
4	8	0.5	Eddy driven jet
5	8.5	0.5	Eddy driven jet
6	7.5	1	Eddy driven jet
7	7	1.5	Mixed properties
8	9	0.5	Eddy driven jet
9	8	1	Eddy driven jet
10	9.5	0.5	Mixed properties
11	10	0.5	Mixed properties
12	7.5	1.5	Mixed properties
13	8.5	1	Mixed properties
14	10	1	Merged jet
15	9	1	Merged jet
16	7	2	Merged jet
17	9.5	1	Merged jet
18	8	1.5	Merged jet
19	8.5	1.5	Merged jet
20	9	1.5	Merged jet
21	7.5	2	Merged jet
22	8.5	2	Merged jet
23	9.5	1.5	Subtropical jet
24	9	2	Subtropical jet
25	10	1.5	Subtropical jet
26	9.5	2	Subtropical jet
27	10	2	Subtropical jet

Earth System
Dynamics
Discussions
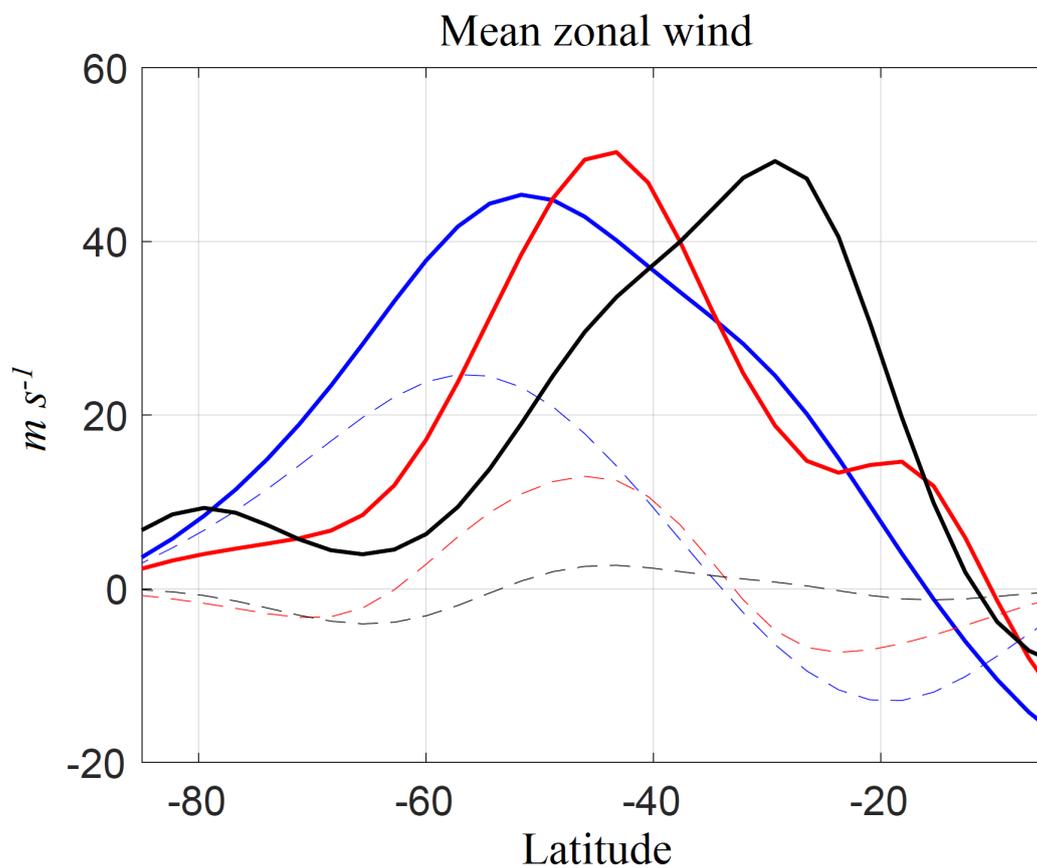
Open Access

Figure A1. Zonal mean zonal wind ($m\ s^{-1}$) in the upper layer ($\overline{u}_u$, thick solid lines) and lower layer ($\overline{u}_l$, thin dashed lines) of the 2-layer QG model, for simulation number 1 from the eddy-driven jet regime (blue lines), simulation number 20 from the merged jet regime (red lines) and simulation number 27 from the subtropical jet regime (black lines). See Table A1 for the parameters of the simulations.